MODELING OF NIP PRESSURES AND WEB FEED RATES IN RUBBER COVERED NIP ROLLERS

By

Kevin Cole
Optimation Technology, Inc.
USA

ABSTRACT

Nip rollers are used extensively in converting processes; however, correct design and usage of these types of rollers requires a sound understanding of the mechanics of the nip in both the machine and cross-width directions. This behavior is difficult to predict owing to the nonlinear nature of the contact region and the near incompressible material characteristics of typical nip roller coverings. This paper is a companion to a paper presented at IWEB11 where experimental data characterizing web feed rates, nip pressures and wrinkling in nip rollers comprised of single and dual durometer cover systems was presented. In this paper, modeling techniques are developed for predicting nip pressures and nip roller feed rates in both the machine and cross-width directions. The models presented include the ability to analyze roller coverings engineered with the ability to control nip roller feed rate while retaining desirable nip pressure characteristics. Parametric studies demonstrating the influence of many of the material and design parameters of nip rollers on nip roller feed rate and nip pressure are presented. Nondimensionalized parameters are also developed to assist engineers in the design of nip rollers to insure suitable performance.

NOMENCLATURE

e	dilatation, equal to $\varepsilon_x + \varepsilon_y$
k_r	foundation stiffness, constant
p	mean stress, equal to $-\frac{1}{3}\left(\sigma_{xx}+\sigma_{yy}+\sigma_{zz}\right)$
p	layer number
r	equivalent nip roller radius, equal to $\frac{r_1 r_2}{r_1+r_2}$
s	response array, equal to $\{u^\alpha, v^\alpha, \sigma_{yy}^\alpha, \sigma_{xy}^\alpha\}$
t	layer thickness
u, v	inplane horizontal and vertical displacements
w	axial half length of nip roller covering

x'	point interpolation function is centered about
A^p	individual elastic layer transfer matrix in multiple layer configuration
A_{ij}, G_{ij}	individual terms of single, multi elastic layer transfer matrix
B	nip roller journal length
$\bar{B}(\alpha)$	term relating periodic normal load to periodic horizontal displacement
$\hat{B}(\alpha)$	term relating periodic normal load to periodic vertical displacement
E	Young's modulus
EI	nip roller shell flexural stiffness
F	complete elastic layer transfer matrix in multiple layer configuration
F_I	interpolation function
$\bar{F}_I(\alpha)$	interpolation function spatial frequency spectrum
I_{11}, I_{21}	influence coefficients representing vertical, horizontal displacement at one point due to a unit load at another point
N, M	response, load point of the influence coefficients
P	total number of layers
$2\pi\alpha^{-1}$	spatial wavelength of loading and displacement response
δ	axial direction nip engagement
δ_i	nip engagement intercept for linearized foundation stiffness
δ_0	nip engagement
ε	roller creep, see reference [1]
$\varepsilon_x, ...$	strain components
η	roller deflection stiffness parameter, equal to $\sqrt[4]{\frac{k_r}{4EI}}$
κ	material constant, defined as $3 - 4\upsilon$, equal to $\frac{\lambda+3\mu}{\lambda+\mu}$ where λ is 1st Lamé constant
σ_0	interpolation function value at $x = x'$
$\sigma_{xx}, ...$	stress components
μ	2nd Lamé constant (shear modulus), equal to $\frac{E}{2(1+\upsilon)}$
υ	Poisson's ratio

INTRODUCTION

Nip rollers are used extensively in the web handling industry for a wide range of applications and generally fall into one of two categories. Web transport deals with web handling processes where the intention is not to permanently deform the web while web processing deals with processes where the intention is to modify the web in some way. While the mechanics of nips in either case tend to be complex owing to nonlinearities of various types, the former case, which is the concern of this paper, is easier to deal with since the nonlinearities generally arise from geometry and not from large strains or material effects.

A companion paper, presented at the 2011 IWEB conference [1], presented results illustrating some of the unique characteristics of nip roller systems and serves as the basis for this paper. The tendency of nip roller systems to convey webs at speeds slightly different than the surface speed outside of the nip was discussed. This effect, referred to as creep, results from the nearly incompressible nature of the rubbers typically used to cover nip rollers. Creep was shown to be a function of nip loading and was demonstrated to give rise to web wrinkling due to cross-direction variation in load arising from nonuniform roller deflection. Methods were described for measuring nip load, nip

engagement, nip footprint and creep. Empirical results were presented for a conventional, single durometer nip roller cover design and for a novel, dual durometer nip roller cover design that provides the ability to control and manage creep so as to reduce the conveyance sensitivity due to differential creep.

The intent of this paper is twofold. First, analytical first principles models will be presented that can be used to study the behavior of nip roller systems that were described previously. Results from the models will be demonstrated and will include comparisons between single and dual durometer systems. The first model, *the nip footprint model*, described at a high level by Timoshenko [2], will serve to develop nip footprint, nip engagement and creep as a function of nip load. Included is the ability to model single or multiple layer rubber covering systems with the added benefit of being able to treat the rubber as being incompressible. The second model, *the nip width model*, serves to enable extension of the nip behavior across the width of the nip roller system and follows the derivation presented by Good [3]. This model will also be applied to the single and dual durometer systems. The second purpose of this paper will be to apply a nondimensional-ization procedure to the nip width model and will be used to bring further understanding to the behavior of nip systems.

NIP MECHANICS FOOTPRINT MODEL

The nip mechanics footprint model presented in this section expands on an approach first described by Timoshenko [2] and consists of several steps: (a) formulation of the governing equations for an elastic layer, (b) derivation of a transfer matrix for analyzing an elastic layer, (c) development of an influence coefficient approach for analyzing one or several layers to arbitrary, finite machine direction load distributions and (d) application of the elastic layer solution to the nip mechanics system.

Step (a) – Governing Equations for an Elastic Layer

In this step, the classical equations for the response of an elastic layer of finite depth are given. Figure 1 shows the stress components which act on an elemental area of an elastic layer. Plane strain is assumed; e.g.., variations in behavior of the layer occur along the layer (x direction – machine direction) and though the layer (y direction – radial direction) but not into the layer (z direction – cross direction). From Figure 1, σ_{xx} and σ_{yy} are the in-plane normal stress components, σ_{zz} is the normal out-of-plane stress component and σ_{xy} is the in-plane shear stress component. The remainder of the stress components are zero. A balance of forces in the x and y directions yields the equilibrium equations:

$$\text{x direction: } \frac{\partial \sigma_{xx}}{\partial x} + \frac{\partial \sigma_{xy}}{\partial y} = 0,$$

$$\text{y direction: } \frac{\partial \sigma_{yy}}{\partial y} + \frac{\partial \sigma_{xy}}{\partial x} = 0. \qquad \{1\}$$
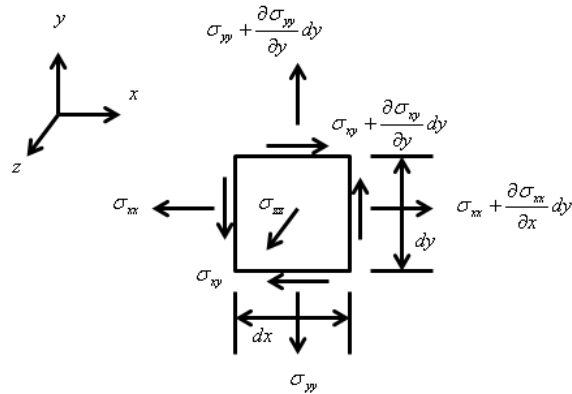
Figure 1 – Elastic Layer Elemental Area, Stress Components

The strain/displacement relationships from Figure 2 are given by:

$$\varepsilon_x = \frac{\partial u}{\partial x}, \quad \varepsilon_y = \frac{\partial v}{\partial y}, \quad \gamma_{xy} = \frac{\partial u}{\partial y} + \frac{\partial v}{\partial x}. \quad \{2\}$$
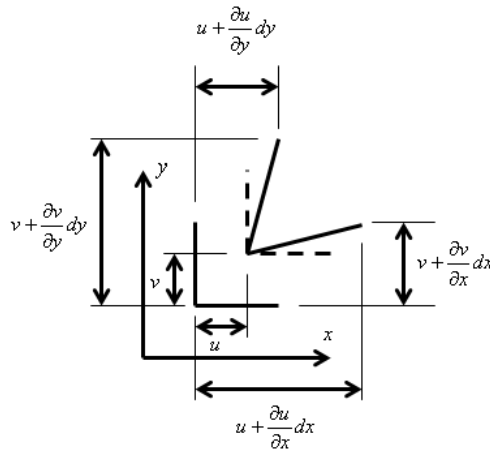

Figure 2 – Elastic Layer Displacement Components

The out-of-plane displacement is zero since variations do not occur in the z direction. We next write equations which relate the stresses and strains. Since the layer is assumed to behave in a linear, elastic manner, Hooke's law applies. Defining the dilatation (expansion in volume per unit volume) as:

$$e \equiv dilatation = \varepsilon_x + \varepsilon_y \quad \{3\}$$

the stress/strain equations are given by:

$$\sigma_{xx} = \frac{3-\kappa}{\kappa-1}\mu e + 2\mu\varepsilon_x$$

$$\sigma_{yy} = \frac{3-\kappa}{\kappa-1}\mu e + 2\mu\varepsilon_y$$

$$\sigma_{zz} = \frac{3-\kappa}{\kappa-1}\mu e, \ \ \sigma_{xy} = \mu\gamma_{xy} \tag{4}$$

In equations {4}, μ and κ are the material properties of the layer and are related to Young's modulus, E, and Poisson's ratio, v, as follows:

$$\kappa = 3 - 4v = \frac{\lambda + 3\mu}{\lambda + \mu}$$

$$\mu = \frac{E}{2(1+v)} \tag{5}$$

Note that κ is introduced to eliminate the first Lamé constant, λ, from the equations as this simplifies subsequent results. Define the mean stress as:

$$p \equiv mean\ stress = -\frac{1}{3}\left(\sigma_{xx} + \sigma_{yy} + \sigma_{zz}\right) \tag{6}$$

From the first three of equations {4}, the dilatation and the mean stress are related by:

$$p = -\frac{\mu(7-\kappa)}{3(\kappa-1)}e = -\frac{\mu(7-\kappa)}{3(\kappa-1)}\left\{\frac{\partial u}{\partial x} + \frac{\partial v}{\partial y}\right\} \tag{7}$$

Substitution of the stress/strain equations into the equilibrium equations with the results expressed in displacements gives Navier's equations:

$$\mu\nabla^2 u + \frac{2\mu}{\kappa-1}\frac{\partial}{\partial x}\left\{\frac{\partial u}{\partial x} + \frac{\partial v}{\partial y}\right\} = 0$$

$$\mu\nabla^2 v + \frac{2\mu}{\kappa-1}\frac{\partial}{\partial y}\left\{\frac{\partial u}{\partial x} + \frac{\partial v}{\partial y}\right\} = 0 \tag{8}$$

If the first of the above equations is differentiated with respect to x and the second with respect to y and the two resulting equations added, we find that the dilatation and mean stress are harmonic, i.e.:

$$\nabla^2 p = 0 \tag{9}$$

where ∇^2 is the Laplacian operator given in rectangular coordinates by:

$$\nabla^2 = \frac{\partial^2}{\partial x^2} + \frac{\partial^2}{\partial y^2} \tag{11}$$

Applying the Laplacian operator to each of the Navier equations shows that the displacements are biharmonic:

$$\nabla^4 u = \nabla^4 v = 0 \tag{12}$$

where the biharmonic operator in rectangular coordinates is given by:

$$\nabla^4 = \frac{\partial^4}{\partial x^4} + \frac{\partial^4}{\partial x^2 \partial y^2} + \frac{\partial^4}{\partial y^4} \tag{13}$$

In the step that follows, equations {12} in conjunction with {4}, {8} and {9} will be used to develop the general displacement solution for a single layer. Before proceeding, it should be noted that this approach is applicable for any value of Poisson's ratio including 0.5. This is a consequence of the form of the stress/strain equations given by equations {4} where for each component, the right hand side is separated into dilatational and shear components. In general, alternate formulations do not handle the incompressible case.

Step (b) – Transfer Matrix for Analyzing an Elastic Layer

In this step, the solution to the elastic layer equations is given. The solution takes the form of a transfer matrix which relates the response of the layer at the top surface ($y = t \equiv layer\ thickness$) to that at the bottom surface ($y = 0$). Separation of variables is used to solve the partial differential equation described by equation {12}. To proceed, assume the displacements can be separated as follows:

$$u(x, y) = u^\alpha(y) \sin \alpha x$$

$$v(x, y) = v^\alpha(y) \cos \alpha x \tag{14}$$

The validity of the separation depends on a corresponding separation of the stress components σ_{yy} and σ_{xy} given by:

$$\sigma_{xy}(x, y) = \sigma_{xy}^\alpha(y) \sin \alpha x$$

$$\sigma_{yy}(x, y) = \sigma_{yy}^\alpha(y) \cos \alpha x \tag{15}$$

As will be shown, these forms are fully consistent with the equations derived in step a. The parameter α (divided by 2π) in these equations represents the spatial frequency of the loading and displacement response. Thus, the loading is assumed to be infinite in extent in the x direction. In step c, Fourier analysis will be used to develop a technique to examine the behavior of the elastic layer when the loading is finite. We are concerned here, however, with the solution for a single, arbitrary value of α. Substitution of equation {14} into equation {12} yields:

$$\left(\frac{d^4 u^\alpha}{dy^4} - 2\alpha^2 \frac{d^2 u^\alpha}{dy^2} + \alpha^4 u^\alpha \right) \sin \alpha x = 0$$

$$\left(\frac{d^4 v^\alpha}{dy^4} - 2\alpha^2 \frac{d^2 v^\alpha}{dy^2} + \alpha^4 v^\alpha \right) \cos \alpha x = 0 \tag{16}$$

The bracketed term must be identically equal to zero to satisfy the equality. The general solution for each case is given by:

$$u^\alpha = a_1 \cosh \alpha y + a_2 \sinh \alpha y + a_3 y \cosh \alpha y + a_4 y \sinh \alpha y$$

$$v^\alpha = b_1 \cosh \alpha y + b_2 \sinh \alpha y + b_3 y \cosh \alpha y + b_4 y \sinh \alpha y \tag{17}$$

We now wish to determine each of the coefficients. Substituting u^α and v^α into equation {9} yields:

$$b_4 = -a_3, \quad b_3 = -a_4, \tag{18}$$

while substituting u^α and v^α into equation {8} yields after much algebra:

$$b_2 = -a_1 + \frac{a_4}{\alpha}\kappa, \quad b_1 = -a_2 + \frac{a_3}{\alpha}\kappa. \tag{19}$$

Collecting results gives for u^α and v^α:

$$u^\alpha = a_1 \cosh \alpha y + a_2 \sinh \alpha y + a_3 y \cosh \alpha y + a_4 y \sinh \alpha y$$

$$v^\alpha = -a_1 \sinh \alpha y - a_2 \cosh \alpha y - a_3 \left\{ y \sinh \alpha y - \frac{\kappa}{\alpha} \cosh \alpha y \right\}$$

$$-a_4 \left\{ y \cosh \alpha y - \frac{\kappa}{\alpha} \sinh \alpha y \right\} \tag{20}$$

To solve for a_1 through a_4 we relate the behavior at the top of the layer ($y = t$) to that at the bottom of the layer ($y = 0$). In our application, we are interested in surface displacements $u^\alpha(y = t) \equiv u^{\alpha t}$ and $v^\alpha(y = t) \equiv v^{\alpha t}$ arising from surface loads $\sigma_{yy}^\alpha(y = t) \equiv \sigma_{yy}^{\alpha t}$ and $\sigma_{xy}^\alpha(y = t) \equiv \sigma_{xy}^{\alpha t}$. These are the variables which we wish to relate to their corresponding values at $y = 0$. To do this the stress components must first be expressed in terms of a_1 through a_4. Substitution of equations {20} into the second and fourth of equations {4} gives the relationships:

$$\sigma_{xy}^\alpha = \mu\{a_1(2\alpha \sinh \alpha y) + a_2(2\alpha \cosh \alpha y) + a_3(2\alpha y \sinh \alpha y - [\kappa - 1]\cosh \alpha y)$$

$$+a_4(2\alpha y \cosh \alpha y - [\kappa - 1]\sinh \alpha y)\}$$

$$\sigma_{yy}^\alpha = \mu\{a_1(-2\alpha \cosh \alpha y) + a_2(-2\alpha \sinh \alpha y) + a_3([\kappa + 1]\sinh \alpha y - 2\alpha y \cosh \alpha y)$$

$$+a_4([\kappa + 1]\cosh \alpha y - 2\alpha y \sinh \alpha y)\} \tag{21}$$

At the bottom of the layer, we now have:

$$u^\alpha(y = 0) \equiv u^{\alpha 0} = a_1$$

$$v^\alpha(y = 0) \equiv v^{\alpha 0} = -a_2 + a_3 \frac{\kappa}{\alpha}$$

$$\sigma_{xy}^\alpha(y = 0) \equiv \sigma_{xy}^{\alpha 0} = 2\mu\alpha a_2 - \mu(\kappa - 1)a_3$$

Inversion of these equations yields the coefficients in terms of the variables at the bottom of the layer:

$$a_1 = u^{\alpha 0}$$

$$a_2 = \frac{\kappa - 1}{\kappa + 1} v^{\alpha o} + \frac{\kappa}{\mu \alpha [\kappa + 1]} \sigma_{xy}^{\alpha 0}$$

$$a_3 = \frac{2\alpha}{\kappa + 1} v^{\alpha o} + \frac{1}{\mu [\kappa + 1]} \sigma_{xy}^{\alpha 0}$$

$$a_4 = \frac{2\alpha}{\kappa + 1} u^{\alpha o} + \frac{1}{\mu [\kappa + 1]} \sigma_{yy}^{\alpha 0} \qquad \{23\}$$

Substitution into equations {20} and {21} gives the transfer matrix relating the value of the variables at the top of the layer to the value of the variables at the bottom of the layer:

$$\begin{Bmatrix} u^{\alpha t} \\ v^{\alpha t} \\ \sigma_{yy}^{\alpha t} \\ \sigma_{xy}^{\alpha t} \end{Bmatrix} = \begin{bmatrix} C + \frac{2\alpha t}{\kappa+1}S & \frac{\kappa-1}{\kappa+1}S + \frac{2\alpha t}{\kappa+1}C & \frac{tS}{\mu[\kappa+1]} & \frac{\kappa S}{\mu\alpha[\kappa+1]} + \frac{tC}{\mu[\kappa+1]} \\ \frac{\kappa-1}{\kappa+1}S - \frac{2\alpha t}{\kappa+1}C & C - \frac{2\alpha t}{\kappa+1}S & \frac{\kappa S}{\mu\alpha[\kappa+1]} - \frac{tC}{\mu[\kappa+1]} & -\frac{tS}{\mu[\kappa+1]} \\ -\frac{4\mu\alpha^2 tS}{\kappa+1} & \frac{4\alpha\mu}{\kappa+1}(S - \alpha tC) & C - \frac{2\alpha t}{\kappa+1}S & -\frac{\kappa-1}{\kappa+1}S - \frac{2\alpha t}{\kappa+1}C \\ \frac{4\alpha\mu}{\kappa+1}(S + \alpha tC) & \frac{4\mu\alpha^2 tS}{\kappa+1} & -\frac{\kappa-1}{\kappa+1}S + \frac{2\alpha t}{\kappa+1}C & C + \frac{2\alpha t}{\kappa+1}S \end{bmatrix} \begin{Bmatrix} u^{\alpha 0} \\ v^{\alpha 0} \\ \sigma_{yy}^{\alpha 0} \\ \sigma_{xy}^{\alpha 0} \end{Bmatrix} \quad \{24\}$$

where $C \equiv \cosh \alpha t$ and $S \equiv \sinh \alpha t$. We now proceed to step c where a Fourier analysis technique is developed which enables loading of finite extent in the x direction to be considered. The technique uses the transfer matrix developed above which considers the behavior of the layer subject to periodic loading of infinite extent in the x direction.

Step (c) – Influence Coefficient Method for Analyzing One or Several Layers

The purpose of this step is to develop a technique whereby the response of the layer to arbitrary, finite load distributions in the x direction can be obtained. To do this, the boundary conditions of the elastic layer must be considered. Suppose that at $y = 0$. the layer is attached to a rigid surface such that $u^{\alpha 0} = v^{\alpha 0} = 0$. Further, assume that at the surface, the only applied load is $\alpha_{yy}^{\alpha t}$ and that the shear load $\alpha_{xy}^{\alpha t} = 0$. Rewriting equation {24} in simplified form as:

$$\begin{Bmatrix} u^{\alpha t} \\ v^{\alpha t} \\ \sigma_{yy}^{\alpha t} \\ \sigma_{xy}^{\alpha t} \end{Bmatrix} = \begin{bmatrix} A_{11} A_{12} A_{13} A_{14} \\ A_{21} A_{22} A_{23} A_{24} \\ A_{31} A_{32} A_{33} A_{34} \\ A_{41} A_{42} A_{43} A_{44} \end{bmatrix} \begin{Bmatrix} u^{\alpha 0} \\ v^{\alpha 0} \\ \sigma_{yy}^{\alpha 0} \\ \sigma_{xy}^{\alpha 0} \end{Bmatrix} \qquad \{25\}$$

we then have from the first two equations of {25}:

$$u^{\alpha t} = A_{13}\sigma_{yy}^{\alpha 0} + A_{14}\sigma_{xy}^{\alpha 0}$$

$$v^{\alpha t} = A_{23}\sigma_{yy}^{\alpha 0} + A_{24}\sigma_{xy}^{\alpha 0} \qquad \{26\}$$

$$\sigma_{yy}^{\alpha t} = A_{33}\sigma_{yy}^{\alpha 0} + A_{34}\sigma_{xy}^{\alpha 0}$$

$$0 = A_{43}\sigma_{yy}^{\alpha 0} + A_{44}\sigma_{xy}^{\alpha 0} \quad\quad \{27\}$$

By inversion:

$$\sigma_{yy}^{\alpha 0} = \frac{A_{44}\sigma_{yy}^{\alpha t}}{A_{33}A_{44} - A_{34}A_{43}}, \quad \sigma_{xy}^{\alpha 0} = -\frac{A_{43}\sigma_{yy}^{\alpha t}}{A_{33}A_{44} - A_{34}A_{43}}. \quad\quad \{28\}$$

Substituting equation {28} into {26} gives:

$$u^{\alpha t} = \frac{A_{13}A_{44} - A_{14}A_{43}}{A_{33}A_{44} - A_{34}A_{43}}\sigma_{yy}^{\alpha t} = \bar{B}(\alpha)\sigma_{yy}^{\alpha t}$$

$$v^{\alpha t} = \frac{A_{23}A_{44} - A_{24}A_{43}}{A_{33}A_{44} - A_{34}A_{43}}\sigma_{yy}^{\alpha t} = \hat{B}(\alpha)\sigma_{yy}^{\alpha t} \quad\quad \{29\}$$

Equation {29} gives the normal and tangential displacements of the layer at the surface when a normal load is applied to the surface. Both the displacements and the applied load are periodic according to equations {14} and {15}. The layer is rigidly attached at the lower boundary and has no applied shear load at the surface.

Equation {29} can be used to determine the response of the layer to arbitrary normal loads. To do this, we introduce the concept of an *interpolating function* and an *influence coefficient*. Suppose an arbitrary load is applied to the elastic layer as shown in Figure 3. Further suppose that we wish to determine the response of the layer at the equally spaced points shown along the surface where some points fall in the load zone and some fall outside the load zone. One way to determine the response is to use the principle of linear superposition. This says that if we know the response to two separately applied loads, then the response when both loads are simultaneously applied is just the sum of the individual responses. Thus, if we decompose the general load into a set of functions, each of the same form but centered at a different point, and determine the response to each load at every point of interest and add them, then we have the general response. A general function which achieves this goal is called an *interpolating function*. The relationship between the load at one point (in this case the interpolating function) and the response at another is called an *influence coefficient*. In this paper, a *Sinc function* has been selected for the interpolating function. It has the following form:

$$interpolating\ function \equiv F_I = \sigma_0(x')\frac{sin\frac{\pi[x-x']}{c}}{\frac{\pi[x-x']}{c}} \quad\quad \{30\}$$

where c is the spacing between interpolation points and x' is the point the interpolating function is centered about. This particular function was selected for several nice features which it possesses. First, arbitrary loading is identically reproduced at each interpolation point since the function is equal to σ_0 at the interpolation point and zero at all others.
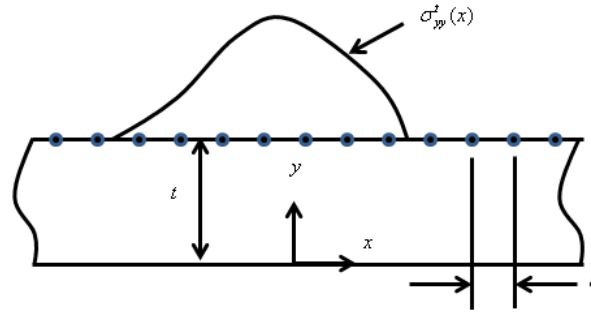
Figure 3 – Arbitrary Finite Normal Load

Thus, at each load point, the particular value of σ_0 is just the value of the arbitrary load at that point. Second, an arbitrary load is very accurately reproduced when several points (10 or more) are used to describe it. To illustrate these features, the decomposition of a parabolic load is presented in Figure 4. Shown in this figure are three approximations to the original curve, each based on the number of points used to interpolate the function. Also shown are the individual interpolation functions for the case where 11 terms were used to approximate the parabolic load. As is indicated and shown in Figure 5, the approximation very closely resembles the original function.

It now remains to determine the response of the layer to the interpolation function (or correspondingly to determine the influence coefficients). For this, we use equation {29} and Fourier analysis. As already described, equation {29} gives the response of the layer to a normal load which is infinite in extent and sinusoidal with spatial frequency, $\alpha/2\pi$. Using Fourier analysis, the interpolating function can be readily decomposed into a finite spatial frequency spectrum. Multiplying this frequency spectrum by the response given by $\bar{B}(\alpha)$ and $\hat{B}(\alpha)$ in equation {29} and integrating over the finite frequency range then yields the general response of the layer to the interpolating function. These ideas are developed mathematically as follows. First, the interpolating function is expanded in a Fourier cosine integral (since the Sinc function is even or symmetric about $x = x'$):

$$F_I(x - x') = \int_0^\infty \bar{F}_I(\alpha) \cos \alpha \, (x - x') d\alpha \qquad \{31\}$$

where from the inverse Fourier cosine integral the Fourier spectrum is:

$$\bar{F}_I(\alpha) = \frac{2}{\pi} \int_0^\infty F_I(x^* - x') \cos \alpha \, (x^* - x') dx^* \qquad \{32\}$$

$$\bar{F}_I(\alpha) = \frac{c\sigma_0}{\pi} \begin{cases} 0 \text{ if } \alpha > \frac{\pi}{c} \\ \frac{1}{2} \text{ if } \alpha = \frac{\pi}{c} \\ 1 \text{ if } \alpha < \frac{\pi}{c} \end{cases} \qquad \{33\}$$
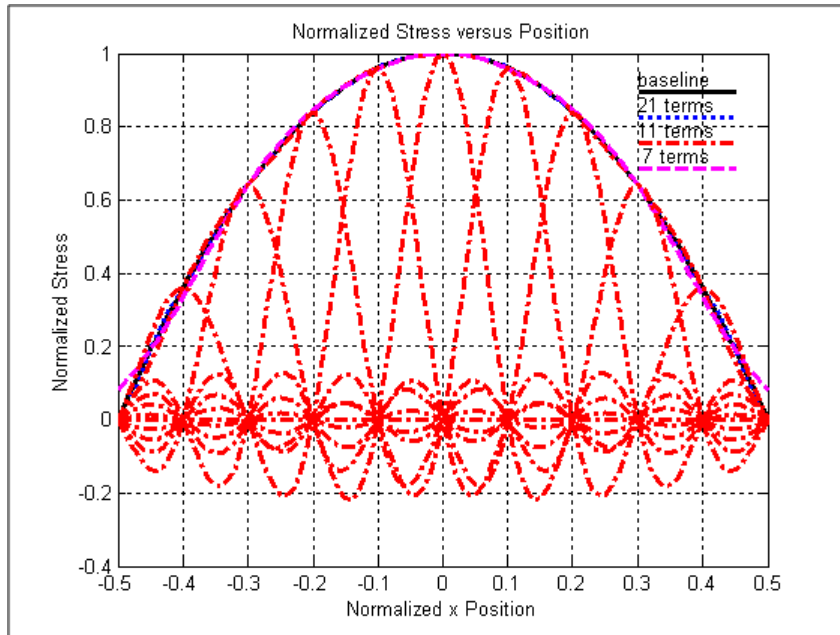
326

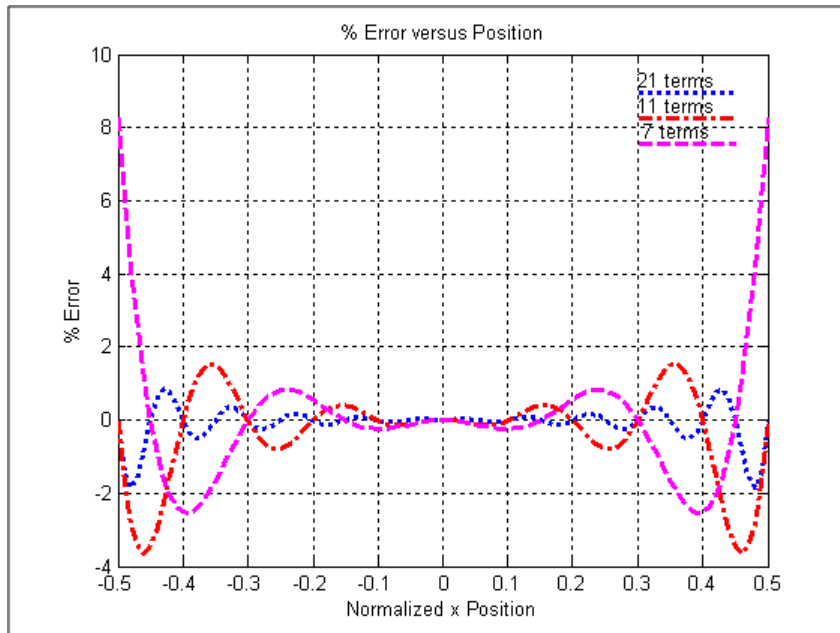Figure 4 – Decomposition of a Normal Load Using the Sinc Function

Figure 5 – %Error Using the Sinc Function

Thus, the spectrum of the interpolating function is finite and further is constant over its nonzero region. In equation {29}, σ_{yy}^{at} can be considered as representing a discrete point of the interpolating function spectrum and the left hand side the corresponding response.

To obtain the response to the entire spectrum, integration according to the form of equation {14} gives:

$$u(x - x', t) = \frac{c\sigma_0}{\pi} \int_0^{\frac{\pi}{c}} \bar{B}(\alpha) \sin \alpha (x - x') d\alpha$$

$$v(x - x', t) = \frac{c\sigma_0}{\pi} \int_0^{\frac{\pi}{c}} \hat{B}(\alpha) \cos \alpha (x - x') d\alpha \qquad \{34\}$$

Equation {34} gives the response at any point x when the interpolating function is centered at $x = x'$. The influence coefficients representing the displacements at one point due to a unit normal load at another are given by:

$$I_{11}(x, x') \equiv I_{11}(M, N) = \frac{v(x - x', t)}{\sigma_0} = \frac{c}{\pi} \int_0^{\frac{\pi}{c}} \hat{B}(\alpha) \cos \alpha (x - x') d\alpha$$

$$I_{21}(x, x') \equiv I_{21}(M, N) = \frac{u(x - x', t)}{\sigma_0} = \frac{c}{\pi} \int_0^{\frac{\pi}{c}} \bar{B}(\alpha) \sin \alpha (x - x') d\alpha \qquad \{35\}$$

where $x = cM$ and $x' = cN$ and M and N are integers representing the locations of the response and load points respectively.

We now have attained the goal of this step; i.e., creating influence coefficients for the elastic layer. The influence coefficients can now be used to form the elements in a general matrix which relates displacements and loads at the surface of the layer. This is the mathematical implementation of the principle of linear superposition. Using this approach, arbitrary loads can be applied to the layer and its corresponding behavior determined. In the next step, we will show how these concepts are used to solve for nip load, nip footprint and creep in terms of nip engagement.

Before proceeding, we first note that up to now, only one layer has been considered. If however, there are many layers, the approach described above is easily extended. In fact, the only change is in the form of $\bar{B}(\alpha)$ and $\hat{B}(\alpha)$. Suppose we have multiple layers which are attached at the interfaces and satisfy the same boundary conditions at the inner and outer surfaces as before $\{(u^{\alpha 0})^1 = (v^{\alpha 0})^1 = 0$ and $(\sigma_{xy}^{\alpha t p})^P\}$. The additional indice denotes the layer location and thickness. The geometry for this case is shown in Figure 6. Each layer will now have its own transfer matrix similar to the form of equation {25} and written in matrix form as:

$$\{s\}^{tp} = [A]^p \{s\}^{0p} \qquad \{36\}$$

where s is the array of responses $u^\alpha, v^\alpha, \sigma_{yy}^\alpha$ and σ_{xy}^α, A is the transfer matrix and p identifies the particular layer across which the transfer matrix acts. In order to get the
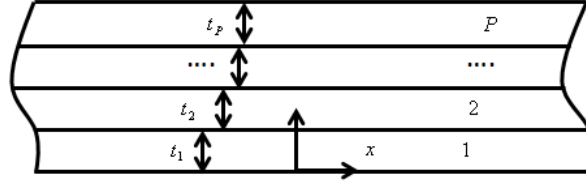
Figure 6 – Multiple Layer Elastic Strip

complete transfer matrix from the bottom of the first layer to the top of the outermost layer, we use matrix multiplication to give:

$$\{s\}^{tP} = [A]^P [A]^{P-1} \dots [A]^2 [A]^1 \{s\}^{01} \equiv [G]\{s\}^{01} \qquad \{37\}$$

From the first two equations of $\{37\}$:

$$(u^{\alpha t})^P = G_{13}(\sigma_{yy}^{\alpha 0})^1 + G_{14}(\sigma_{xy}^{\alpha 0})^1$$

$$(v^{\alpha t})^P = G_{23}(\sigma_{yy}^{\alpha 0})^1 + G_{24}(\sigma_{xy}^{\alpha 0})^1 \qquad \{38\}$$

Following similar steps used to derive equation $\{28\}$, we find the stress components at $y = 0$ in terms of the nominal stress at $y = t_1 + t_2 + \dots + t_{P-1} + t_P$:

$$(\sigma_{yy}^{\alpha 0})^1 = \frac{G_{44}(\sigma_{yy}^{\alpha t})^P}{G_{33}G_{44} - G_{34}G_{43}}, \quad (\sigma_{xy}^{\alpha 0})^1 = -\frac{G_{43}(\sigma_{yy}^{\alpha t})^P}{G_{33}G_{44} - G_{34}G_{43}}. \qquad \{39\}$$

Substitution of equation $\{39\}$ into $\{38\}$ yields:

$$(u^{\alpha t})^P = \frac{G_{13}G_{44} - G_{14}G_{43}}{G_{33}G_{44} - G_{34}G_{43}}(\sigma_{yy}^{\alpha t})^P = \bar{B}(\alpha)(\sigma_{yy}^{\alpha t})^P$$

$$(v^{\alpha t})^P = \frac{G_{23}G_{44} - G_{24}G_{43}}{G_{33}G_{44} - G_{34}G_{43}}(\sigma_{yy}^{\alpha t})^P = \hat{B}(\alpha)(\sigma_{yy}^{\alpha t})^P \qquad \{40\}$$

The components of the complete transfer matrix G are given by:

$$G_{ij} = \sum_{k=1}^4 A_{ik}^P \sum_{l=1}^4 A_{kl}^{P-1} \sum_{m=1}^4 A_{lm}^{P-2} \dots \sum_{\beta=1}^4 A_{\gamma\beta}^3 \sum_{\lambda=1}^4 A_{\beta\lambda}^2 \, A_{\lambda j}^1 \qquad \{41\}$$

The influence coefficients for the multiple layer response can now be calculated using equation $\{35\}$ where the form of $\bar{B}(\alpha)$ and $\hat{B}(\alpha)$ is given in Equation $\{40\}$.

Step (d) – Application of the Elastic Layer Solution to the Nip Mechanics System

In previous steps, a method was derived for analyzing the response of a single or multiple layers to a normal finite distributed load. The solution approach, derived in rectangular coordinates, uses a matrix of influence coefficients which relate the surface displacements to the surface normal loads. In order to adapt this solution to the nip mechanics problem, we use the fact that for small displacements, geometric equivalence can be developed between the elastic layer formulation and the nip roller system.

response of these two rollers under vertical loading can be developed from the solutions presented in the previous sections by imposing geometric compatibility and normal stress boundary conditions that exist in the nip roller system onto the elastic layer solution. Consider the system to be loaded such that the two nip rollers engage by an amount δ^0.
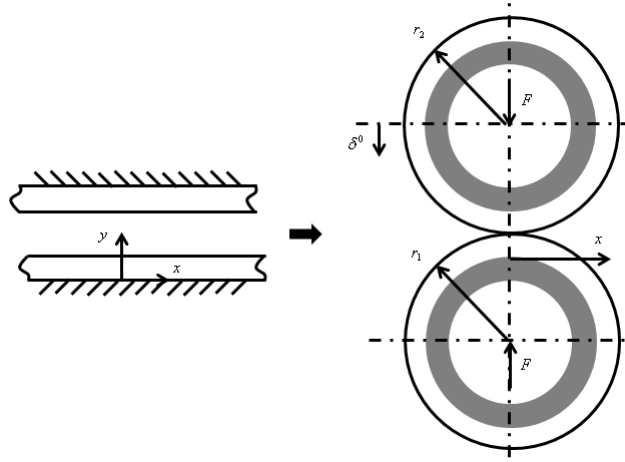

Figure 7 – Geometric Equivalence between Elastic Layer and Nip Roller System

From geometry, the amount of engagement will be a function of x in the nip zone and can be expressed as:

$$\delta(x) = \delta^0 - \frac{x^2}{2r_1} - \frac{x^2}{2r_2} = \delta^0 - \frac{x^2}{2r} \tag{42}$$

where r equals the equivalent radius and is given by:

$$r = \frac{r_1 r_2}{r_1 + r_2} \tag{43}$$

Inside of the nip zone, the vertical displacement of the two layers at the surface will be equivalent to the nip engagement and the normal forces will be equal:

$$\{\delta(x)\} = v_1^{tP}(x) + v_2^{tP}(x), \quad \sigma_{yy1}^{tP}(x) = \sigma_{yy2}^{tP}(x), \tag{44}$$

where the integer subscripts refer to roller number. Outside of the nip, the normal stresses will be equal to zero:

$$\sigma_{yy1}^{tP}(x) = \sigma_{yy2}^{tP}(x) = 0 \tag{45}$$

Dispensing with the subscripts and superscripts while retaining subscripts indicating roller number, we can now write the results from equation {35} into matrix form as:

$$\begin{Bmatrix} v \\ u \end{Bmatrix}_{1,2} = \begin{bmatrix} I_{11} & I_{12} \\ I_{21} & I_{22} \end{bmatrix} \begin{Bmatrix} \sigma_{yy} \\ \tau_{xy} \end{Bmatrix}_{1,2} \tag{46}$$

330

Our solution derived in step c has determined I_{11} and I_{12}. The influence coefficients resulting from a unit shear load have not been derived but could be following the same procedure as outlined in step c.

We now use the boundary conditions in combination with the influence coefficient matrix to solve for nip footprint, nip load and creep in terms of nip engagement. To proceed, we recognize that we only need to consider the first relationship in matrix equation {46}:

$$\{v\}_{1,2} = [I_{11}]_{1,2}\{\sigma_{yy}\}_{1,2} \qquad \{47\}$$

We now partition normal displacements and loads into two components – those in the nip and those outside of the nip:

$$\{v\}_{1,2} = \{v_{in}\}_{1,2}, \{v_{out}\}_{1,2} \qquad \{48\}$$

$$\{\sigma_{yy}\}_{1,2} = \{(\sigma_{yy})_{in}\}_{1,2}, \{(\sigma_{yy})_{out}\}_{1,2} \qquad \{49\}$$

Substitution of these into Equation {45} yields the expanded form for the 1,1 component:

$$\left\{ \begin{matrix} v_{in} \\ v_{out} \end{matrix} \right\}_{1,2} = \begin{bmatrix} I_{11}^1 & I_{11}^2 \\ I_{11}^3 & I_{11}^4 \end{bmatrix} \left\{ \begin{matrix} (\sigma_{yy})_{in} \\ (\sigma_{yy})_{out} \end{matrix} \right\}_{1,2} \qquad \{50\}$$

Expansion of equation {50} gives:

$$\{v_{in}\}_{1,2} = [I_{11}^1]_{1,2}\{(\sigma_{yy})_{in}\}_{1,2} \qquad \{51\}$$

$$\{v_{out}\}_{1,2} = [I_{11}^3]_{1,2}\{(\sigma_{yy})_{in}\}_{1,2} \qquad \{52\}$$

Equation {51} can be inverted:

and the second nip boundary condition used to develop a relationship between the normal displacements at the surface of the outermost layers of each roller:

$$[I_{11}^1]_1^{-1}\{v_{in}\}_1 = [I_{11}^1]_2^{-1}\{v_{in}\}_2 \qquad \{54\}$$

This expression can be solved for the normal displacements at the outermost layer of the first roller in terms of the second:

$$\{v_{in}\}_1 = [I_{11}^1]_1[I_{11}^1]_2^{-1}\{v_{in}\}_2 \qquad \{55\}$$

We now apply the first nip boundary condition to give:

$$\{\delta(x)\} = [I_{11}^1]_1[I_{11}^1]_2^{-1}\{v_{in}\}_2 + \{v_{in}\}_2 = \{[I_{11}^1]_1[I_{11}^1]_2^{-1} + [\because]\}\{v_{in}\}_2 \qquad \{56\}$$

where $[\because]$ is the identity matrix. This equation can now be inverted to yield the normal displacements at the outermost layer of the second roller:

$$\{v_{in}\}_2 = \{[I_{11}^1]_1[I_{11}^1]_2^{-1} + [\because]\}^{-1}\{\delta(x)\} \qquad \{57\}$$

Back substitution into equation {55} gives the displacements of the first roller:

$$\{v_{in}\}_1 = [I_{11}^1]_1[I_{11}^1]_2^{-1}\{[I_{11}^1]_1[I_{11}^1]_2^{-1} + [\because]\}^{-1}\{\delta(x)\} \qquad \{58\}$$

The normal loads can be found from equation {55} and the normal displacements at the outermost layers of both rollers outside of the nip from equation {52}. The tangential displacements within the nip region can be found from the second relationship of matrix equation {46} where the I_{21} is partitioned similar to I_{11}:

$$\{u_{in}\}_{1,2} = [I_{21}^1]_{1,2}\{(\sigma_{yy})_{in}\}_{1,2} \qquad \{59\}$$

Finally, the x direction displacements can be differentiated and averaged through the nip region to give an approximate estimate of creep (ε as defined in reference [1]):

where A is the nip width [1]. The tangential strain, $\frac{\partial u}{\partial x} = \varepsilon_x$, is computed using a finite difference approximation accurate to second order:

$$\left(\frac{\partial u}{\partial x}\right)_{1,2} = \frac{u_{in,1,2}(x+c) - u_{in,1,2}(x-c)}{2c} \qquad \{61\}$$

For a given amount of nip engagement, equations {57} and {58} are used to compute normal displacements at the outermost surfaces of rollers 1 and 2 inside of the nip. Equation {53} is used to compute the normal loads while equation {60} is used to compute the creep. Since the nip width is not known a priori as a function of nip engagement, the solution must be obtained iteratively by guessing a point where the nip ends and then calculating loads in the nip and normal displacements outside of the nip. If either condition is violated (e.g., loads are tensile in the nip or normal displacements outside of the exceed the geometric limit imposed by equation {42}), the end point is appropriately modified and loads and normal displacements recomputed. This process continues until both sets of boundary conditions are satisfied.

The entire process described in steps (a) through (d) has been programmed to enable computation of nip footprint, nip load and creep as a function of nip engagement for user specified material and geometric inputs. The program allows the nip roller cover to have up to eight layers with independent material (Young's modulus and Poisson's ratio up to 0.5) and geometric (thickness) properties.

Results from the new model are shown in Figure 8 through 10. Inputs to the model can be found in Table 1and Table 2 (systems 1 and 2) from reference [1]. Figure 8 presents nip
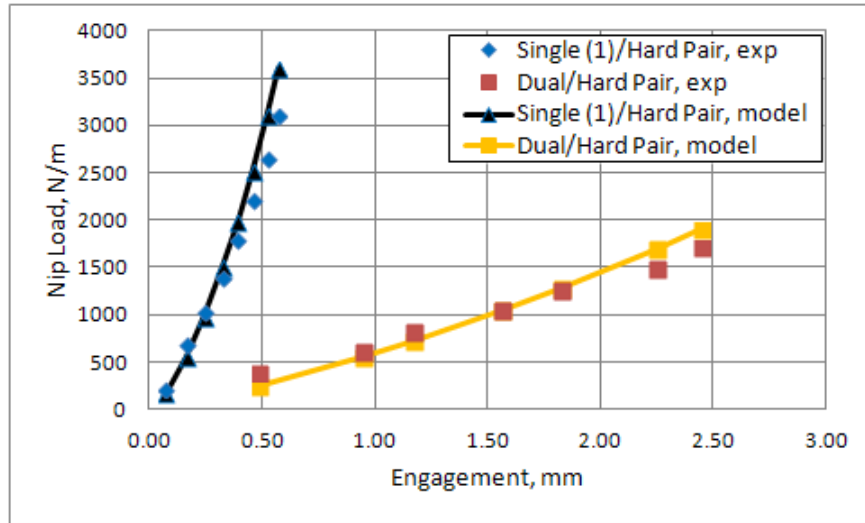
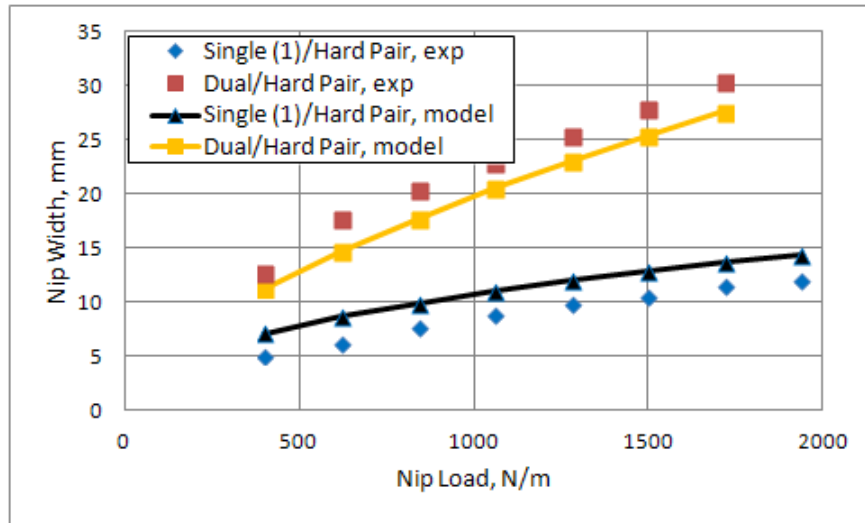Figure 8 – Nip Load vs. Engagement, Model vs. Experiment

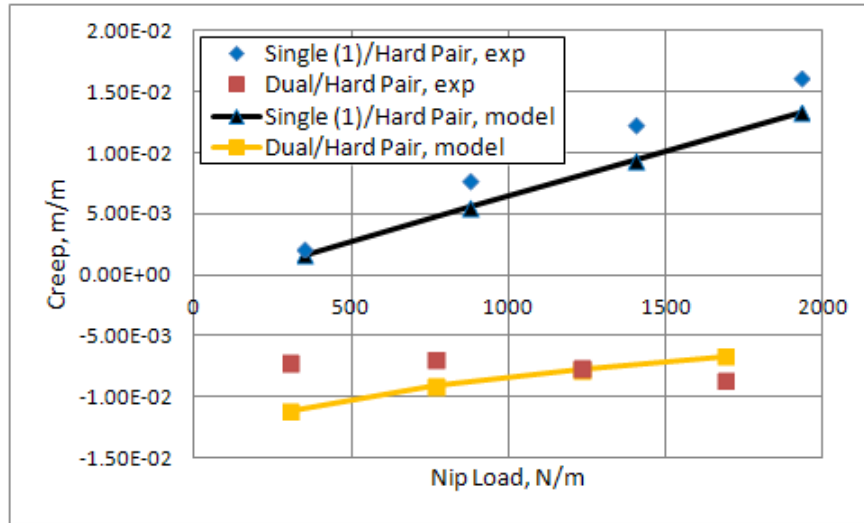Figure 9 – Nip Width vs. Nip Load, Model vs. Experiment

Figure 10 – Creep vs. Nip Load, Model vs. Experiment

load versus engagement, Figure 9 presents nip width versus nip load and Figure 10 presents creep versus nip load. In each case, comparisons between theory and experiment are presented for two systems (single layer/hard roller and dual durometer [2 layers]/hard roller). Very good agreement is seen in all cases between the experiment and model results.

NIP WIDTH MODEL

The purpose of this section is to investigate the behavior of the nip roller system in the axial direction. The intent is to build off of work previously reported by Good [3] where his results indicated that a two dimensional formulation that treats the stiffness of the rubber coverings as a Winkler foundation and the deflection of the roller shells as an Euler beam provides an excellent framework to study the axial behavior of a nip system. In this paper, a model that incorporates these features was derived by developing and solving the governing fourth order differential equation:

$$\frac{d^4\delta}{dz^4} + \frac{k_r}{EI}\delta = \frac{k_r}{EI}\delta_i \qquad \{62\}$$

subject to appropriate boundary conditions (see Figure 11 for system geometry):

$$at\ z = 0, moment = -FB \rightarrow \frac{d^2\delta}{dz^2}(z = 0) = \frac{FB}{EI}$$

$$at\ z = 0, shear = F \rightarrow \frac{d^3\delta}{dz^3}(z = 0) = \frac{F}{EI}$$

$$at\ z = w, slope = 0 \rightarrow \frac{d\delta}{dz}(z = w) = 0$$

$$at\ z = w, shear\ force = 0 \rightarrow \frac{d^3\delta}{dz^3}(z = w) = 0 \qquad \{63\}$$
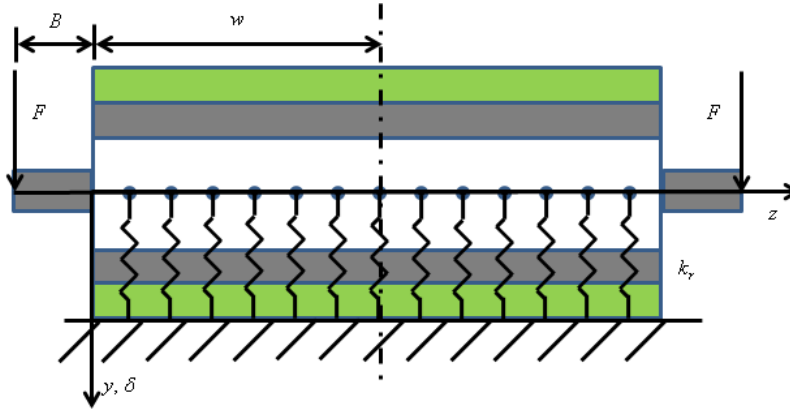

Figure 11 – Analytic Model of a Rubber Covered Roller System

The foundation stiffness can be determined from the previous solution and can be approximated by linearizing about the nominal average distributed load, $q = F/w$. This approach simplies the analysis while still retaining the ability to develop a more detailed understanding of the behavior of the nip system. The solution to the differential equation takes the following form:

$$\delta(z) = e^{\eta z}\{g_1 \cos \eta z + g_2 \sin \eta z\} + e^{-\eta z}\{g_3 \cos \eta z + g_4 \sin \eta z\} + \delta_i \qquad \{64\}$$

where $\eta = \sqrt[4]{\frac{k_r}{4EI}}$ is a parameter that represents the relative contribution of the rubber stiffness versus the flexural rigidity of the shell and the coefficients are constants of integration. It should be noted that this model can simulate a wide range of scenarios including the cases considered in the previous section. Application of the boundary conditions yields the following matrix expression for the integration constants (where $c \equiv \cos \eta w$ and $s \equiv \sin \eta w$):

$$\begin{bmatrix} 0 & 2\eta^2 & 0 & -2\eta^2 \\ -2\eta^3 & 2\eta^3 & 2\eta^3 & 2\eta^3 \\ \eta e^{\eta w}(c-s) & \eta e^{\eta w}(c+s) & -\eta e^{-\eta w}(c+s) & \eta e^{-\eta w}(c-s) \\ -2\eta^3 e^{\eta w}(c+s) & 2\eta^3 e^{\eta w}(c-s) & 2\eta^3 e^{-\eta w}(c-s) & 2\eta^3 e^{-\eta w}(c+s) \end{bmatrix} \begin{Bmatrix} g_1 \\ g_2 \\ g_3 \\ g_4 \end{Bmatrix} = \begin{Bmatrix} \frac{FB}{EI} \\ \frac{F}{EI} \\ 0 \\ 0 \end{Bmatrix} \qquad \{65\}$$

Equation {65} can be inverted to give the integration constants from which the final solution can be written by substitution into equation {64}. For the work that follows, two metrics of interest are defined: (a) $delta\ displacement \equiv \delta_{del} = \delta(0) - \delta(w)$ and (b) $average\ displacement \equiv \delta_{ave} = \frac{\delta(0)+\delta(w)}{2}$:

$$\delta_{del} = \{1 - e^{\eta w}c\}g_1 - e^{\eta w}sg_2 + \{1 - e^{-\eta w}c\}g_3 - e^{-\eta w}sg_4 \qquad \{66\}$$

$$\delta_{ave} = \frac{\{1+e^{\eta w}c\}g_1 + e^{\eta w}sg_2 + \{1+e^{-\eta w}c\}g_3 + e^{-\eta w}sg_4}{2} + \delta_0 \qquad \{67\}$$

Others can be chosen but these are adequate to illustrate our analysis method. With the solution in hand, we now desire a way to investigate the behavior of the system in a more systematic way. For this purpose, we appeal to dimensional analysis as a means to identify the minimum number of nondimensional groupings of the variables of the problem. Following procedures presented by Szirtes [4], we determine that since there are six dimensional variables (e.g., δ_{del} or $\delta_{ave}, w, B, \eta, EI, F$) and two dimensions (e.g., N, m), there must therefore be four linearly independent products of dimensional variables. Following Szirtes [4], we find the following four to be especially useful:

$$\pi_1 = \frac{\delta_{del}}{w}\ or\ \frac{\delta_{ave}}{w},\ \pi_2 = \frac{B}{w},\ \pi_3 = \eta w,\ \pi_4 = \frac{EI}{Fw^2} \qquad \{68\}$$

The set of nondimensional variables given by equation {68} is complete meaning that since there is a relation between the physical variables:

$$\psi_1\{\delta_{del}\ or\ \delta_{abs}, w, B, \eta, EI, F\} = constant \qquad \{69\}$$

$$\psi_2\{\pi_1, \pi_2, \pi_3, \pi_4\} = constant \qquad \{70\}$$

We can simplify equation {70} by recognizing from the solutions presented in equations {66} and {67} that the displacements are linear functions of loading and thus the constant in equation {70} is equal to zero and further:

$$\pi_1 = \pi_4^{-1}\psi_2\{\pi_2, \pi_3\} \qquad \{71\}$$

Finally, we have:

$$\pi_1\pi_4 = \psi_2\{\pi_2, \pi_3\} \qquad \{72\}$$

Thus, the dependent variable $\pi_1\pi_4$ is an unknown function of one nondimensional variable, π_3, where π_2 can be treated as a parameter. Equation {72} can be rewritten in terms of dimensional variables as follows (where the average distributed load, $q = \frac{F}{w}$ replaces the end load):

$$\frac{\delta}{q}\frac{EI}{w^4} = \psi_2\left\{\sqrt[4]{\frac{k_r w^4}{4EI}}, \frac{B}{w}\right\} \qquad \{73\}$$

Figures 12 and 13 present results from equation {73} for delta displacement and average displacement as a parametric function of $\pi_2 = \frac{B}{w}$. These results were obtained by solving equations {66} and {67} over the following range of dimensional variables:

$$1.75x10^4 < k_r < 3.5x10^5 \frac{N}{m}, 2.87x10^4 < EI < 2.87x10^5 Nm^2,$$

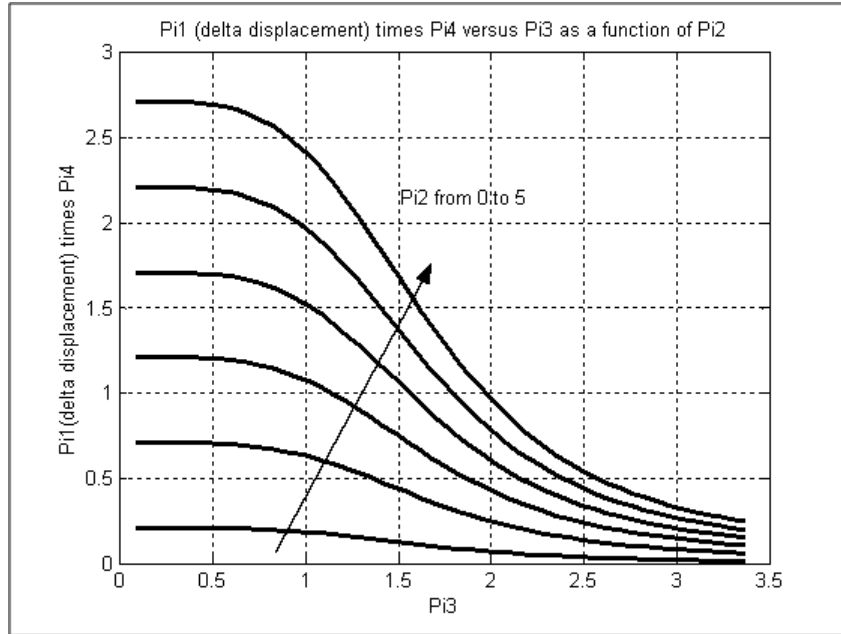$$0.1016 < w < 1.106m, 8.897 < F < 1779N, B = 0, 0.0254, \ldots, 0.127m$$

Figure 12 $- \pi_1(\delta_{del})\pi_4$ versus π_3 as a function of π_2

Figures 12 and 13 concisely present the results for the radial deflection of the nip roller system. Several observations can be seen by careful examination of these two figures. First, relative displacement is affected more significantly by journal length (B) compared to average displacment. This is indicated by the increased spread between curves for the former compared to the later and would be expected as increasing moment at $x = 0$ does not affect the total load. Second, reduction in π_3 (by decreasing the rubber stiffness, k_r) results in a relatively small increase in relative displacement (Figure 12) but a much more significant increase in average displacement (Figure 13). For example, for the two nip roller systems modeled previously, one finds that to achieve the same average displacement in the dual durometer system ($\pi_3 = 0.69$) requires a loading that is 13% of that for the single durometer system ($\pi_3 = 1.21$). Accounting for this reduction in loading results in a delta displacement for the dual durometer system that is 16% of
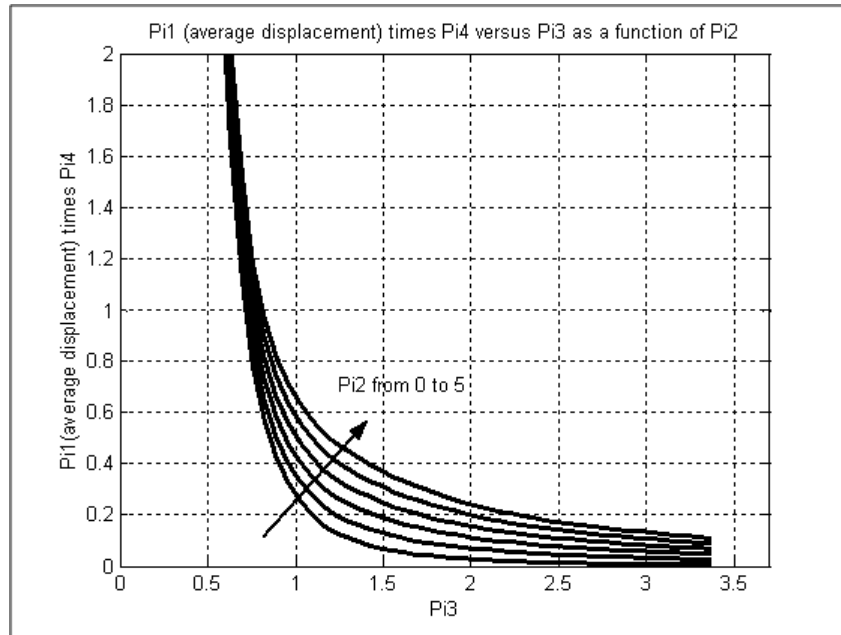
Figure 13 – $\pi_1(\delta_{ave})\pi_4$ versus π_3 as a function of π_2

that of the single durometer system. This assessment assumes that the user desires that the nip system engagement be held constant between the two systems. This might be desired, for example, if the nip process requires constant dwell time for process invariance. Third, it is evident from the two figures that the space the dual durometer system occupies is significantly more flexible compared to the single durometer system. This implies that the axial distribution of nip force is tending to become more uniform. In the limit at $\pi_3 = 0$, it can easily be shown that the constant in Figure 12 becomes equal to $\frac{5}{24} = 0.208$ and that the curves for increasing B increment by 0.5 since this solution is identically equal to that of a uniformly centrally loaded simply supported beam. Observation of Figure 12 confirms that indeed these are the ordinal values at $\pi_3 = 0$.

This methodology is illustrative and can readily be extended to other metrics deemed useful from a design standpoint. Other examples include designing for uniform pressure, minimal creep and minimal differential creep.

CONCLUSIONS

A theoretical model that predicts nip footprint, nip load and creep as a function of nip engagement has been presented. The model is developed by first formulating the exact solution to a linear elastic strip and then using equations of kinematic and force constraint to apply the solution to nip systems. Formulation of the plane strain model in terms of dilatational and deviatoric stress components enables the elastomeric covering material to be modeled as incompressible. It was further demonstrated how to extend the model to coverings comprised of multiple layers. The model was applied to results presented by Cole [1] and correlation between theory and experiment was shown to be very good. An axial effects model was then presented and dimensional analysis used to develop graphical solutions that enable a more coherent means to understand and design

nip roller systems. It was shown that single durometer nip systems occupy a different physical space compared to single durometer systems owing to the increased cover flexibility of one such system. Depending on the requirements of the nip process, this difference must be accounted for to ensure that performance objectives are met.

ACKNOWLEDGEMENTS

REFERENCES

1. Cole, K. A., and Walker, T. J., "Measurement of Web Feed Rates in Rubber Covered Nip Roller Applications and the Impact on Wrinkle Formulation," Proceedings of the 10th International Conference on Web Handling, Oklahoma State University, Stillwater, Oklahoma, June 2011.
2. Timoshenko, S. P., and Goodier, J. N., Theory of Elasticity, McGraw-Hill, 3rd ed., 1970, pp. 53-60.
3. Good, J. K, "Modeling Rubber Covered Nip Rollers in Web Lines," Proceedings of the 6th International Conference on Web Handling, Oklahoma State University, Stillwater, Oklahoma, June 2001, pp. 159-177.
4. Szirtes, T., Applied Dimensional Analysis and Modeling, McGraw-Hill, 1st ed., 1998.